Heydarian, Reza; Klimov, Vasily; Simovski, Constantin

Subwavelength effects near a dielectric microcylinder illuminated by a diffraction-free beam

Published in:
Photonics and Nanostructures: Fundamentals and Applications

DOI:
10.1016/j.photonics.2021.100894

Published: 01/02/2021

Document Version
Publisher's PDF, also known as Version of record

Please cite the original version:
Heydarian, R., Klimov, V., & Simovski, C. (2021). Subwavelength effects near a dielectric microcylinder illuminated by a diffraction-free beam. *Photonics and Nanostructures: Fundamentals and Applications*, *43*, Article 100894. https://doi.org/10.1016/j.photonics.2021.100894

Photonics and Nanostructures - Fundamentals and Applications 43 (2021) 100894

Contents lists available at ScienceDirect

Photonics and Nanostructures - Fundamentals and Applications

journal homepage: www.elsevier.com/locate/photonics

Subwavelength effects near a dielectric microcylinder illuminated by a diffraction-free beam

Reza Heydarian [a,*], Vasily Klimov [b], Constantin Simovski [a,c]

[a] Department of Electronics and Nano-Engineering, Aalto University, P.O. Box 15500, FI-00076 Aalto, Finland
[b] Department of Optics, Lebedev Physical Institute, Russian Academy of Science, 53, Leninsky Prospekt, 119991 Moscow, Russia
[c] Faculty of Physics and Engineering, ITMO University, 199034, Birzhevaya Line 16, Saint-Petersburg, Russia

ARTICLE INFO

Keywords:
Diffraction free beam
Microcylinder
Near field effects

ABSTRACT

Generation of a photonic nanojet with a slightly subwavelength waist at the back side of a dielectric microsphere or microcylinder impinged by a plane wave has recently shown that the near-field effects may hold not only inside the dielectric microparticle, but also outside it. In this paper we explain how to drastically increase the external near-field effect. For it one has to replace a plane wave or a Gaussian beam by the fully symmetric diffraction-free beam. In this case we observe a deeply subwavelength focusing of the incident beam near the rear edge of the microcylinder. This effect is accompanied by a very strong enhancement of the local electric intensity. Microcylinders with slightly different parameters grant the significant enhancement of the intensity on the whole cylinder surface. These implications of the resonant scattering result from the destructive interference of the propagating spatial harmonics which vanish at the back side of the cylinder in favor of the evanescent ones.

1. Introduction and problem formulation

In this paper we theoretically reveal two new near-field effects which when a properly chosen 2D wave beam impinges a dielectric microcylinder with optically large radius $kR \gg \pi$ (here and below $k = 2\pi/\lambda$ is the wave number of free space). Our incident beam is a 2D analogue of the radially polarized Mathieu beam [1] and is called in the theory of diffraction either the 2D Mathieu beam or cosine wave beam [2]. In practice, such a beam results from the transmission of two plane waves [1–12] through a large diaphragm $D \gg \lambda$. These waves have the same frequency and opposite phases and their wave vectors should form a sharp angle 2β as it is depicted in Fig. 1. From the aperture D till the distances exceeding D, the cosine beam experiences the Abbe diffraction only in its tails. In the paraxial domain of the beam only the interference of two plane waves is observed. For our purposes, the presence of the diaphragm is not relevant. In our preliminary simulations, we have seen that the power flux distant from the cylinder lateral edges $x = \pm R$ by $\Delta x > \lambda$ does not feel the presence of the cylinder. The essential part of the incident beam is the interval $-R - \lambda < x < R + \lambda$. For this part of the cosine beam the diaphragm has no impact, and in our study reported below the wave beam is formed simply by two plane waves with the divergence angle 2β between their wave vector $\mathbf{k}^{\pm}$.

If this angle is small enough ($2\beta < \pi/kR$) and the beam is TM-polarized the x-component of the incident electric field and the incident magnetic field grows versus $|x|$ from zero almost linearly over the interval $|x| = [0, R]$. In this case the period of the incident beam intensity versus x is optically large, and the maximal intensity (square of the electric field amplitude) of the incident beam $I_i(x) = I_m$ holds when $|x| > R$. In this paper, we will show that this structure of the incident beam enables very strong near-field effects in the area behind the cylinder and on its surface.

Since the cylinder practically feels the incident beam only within the interval $x = [-R - \lambda, R + \lambda]$ it is reasonable to normalize the electric intensity I of the total field to the intensity I_0 – that of the incident beam averaged namely over this interval. The value I_0 is marked in Fig. 1.

In our study we aim to obtain the subwavelength concentration of the electric field outside the cylinder, i.e. our target is to achieve high values of the local intensity enhancement I/I_0.

Resonant enhancement of the electric intensity at some points inside a dielectric microcylinder is a well-known feature of the resonant scattering theoretically revealed by G. Mie for a sphere 150 years ago and discussed in books for spheres and cylinders, see, e.g. in [3]. Even inside the cylinders the local intensity enhancement may be very high – of the order of 100 [4]. However, the resonant scattering effects that result in

* Corresponding author.
E-mail address: reza.heydarian@aalto.fi (R. Heydarian).

https://doi.org/10.1016/j.photonics.2021.100894
Received 12 November 2020; Received in revised form 14 December 2020; Accepted 8 January 2021
Available online 18 January 2021

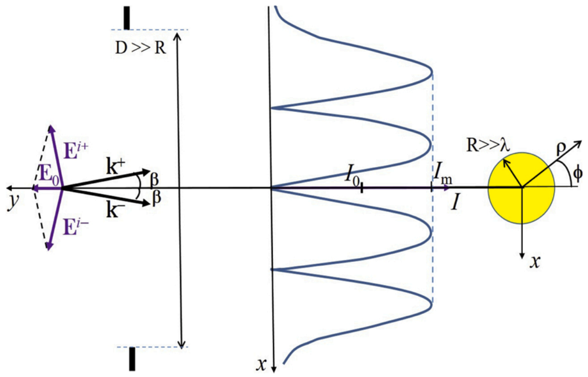

Fig. 1. Planar problem: a cosine beam impinges a dielectric microcylinder. Cartesian and cylindrical coordinates systems are shown, important notations are depicted.

the strong local intensity enhancement outside the cylinder have not been known previously. This enhancement as a rule is fixed in the reflected field and is of the order of 2 even at whispering gallery resonances when the internal enhancement is maximal [3,4]. In the transmitted field – behind the cylinder – the most known effect of enhanced intensity is the waist of the so-called photonic nanojet [5]. A photonic nanojet is a wave beam arising on the back side of a dielectric particle (a microcylinder or a microsphere) illuminated by a plane wave. On the back surface of the microparticle and at a small distance behind it this beam has a waist of subwavelength effective width [5–8]. In the domain of this waist, the electric field comprises a noticeable evanescent-wave component, a longitudinal component of the electric field arises there and the electric intensity enhances several times compared to that of the incident wave [6,8]. However, this known near-field effect is quite weak. For a microsphere, the waist effective width calculated at the rear sphere surface is within the range $(0.29-0.35)\lambda$ [5–8]. For a microcylinder, this width is $(0.4-0.5)\lambda$, whereas the local enhancement of the electric intensity inside the waist does not exceed 4 [8]. At a distance of about 2λ from the microcylinder the Abbe diffraction turns this waist into a usual wave beam of Gaussian type. It is clear, that the generation of the photonic nanojet by a plane wave is such the combination of near-field and far-field effects, in which the far fields dominate.

In this paper we will report the high values of I/I_0 behind the cylinder which have nothing to do with the photonic nanojet. The problem symmetry in Fig. 1 prohibits the generation of the photonic nanojet. On the axis y the total electric field is longitudinal ($E_\rho(\phi=0)=E_y\neq 0$, $E_\phi=0$) and the magnetic field nullifies. Suppressing this way the propagating part of the total field spatial spectrum in the paraxial region our wave beam offers the enhancement to the evanescent components of this spectrum. This point will be additionally discussed below. We will show that the rear point of the cylinder ($x=0$, $y=R$), or, in cylindrical coordinates ($\phi=0$, $\rho=R$), may be a center of a deeply subwavelength focal spot in which amazingly high values of I/I_0 are achieved. This subwavelength field concentration in free space results from the proper choice of the incident wave beam parameters – symmetry shown in Fig. 1 and small angle β (it should be smaller than $\pi/2kR$) – and from the optical thickness of the cylinder $R\gg\lambda$. This subwavelength field concentration is our first new result. Our second result is a high field enhancement in an optically large area – on the whole surface of the cylinder.

2. Calculations: results and discussion

2.1. Subwavelength focusing

In our calculations we use a full-wave commercial solver (COMSOL Multiphysics) and a classical analytical solution of the 2D diffraction problem for a cylinder impinged by a single plane wave [9]. For a single plane wave incident on the optically large cylinder $kR\gg\pi$ this solution (series of the cylindrical functions with cylindrical Mie coefficients of TM type) has no practical meaning – the series converges very slowly. In this case, besides of commercial solvers, one applies high-frequency asymptotics or performs numerical integration in the integral form of the solution (see, e.g. in [9,3]). However, for our incident beam of two plane waves with the symmetric polarization we combine the terms corresponding to $\mathbf{k}^+$ with the terms corresponding to $\mathbf{k}^-$ and obtain a the series of cylindrical functions whose coefficients grant much faster convergence compared to the case of a single plane wave incident along the axis y. This convergence grants us the possibility to simply sum up the terms in the home-made Matlab code until the result nearly stops to change. The comparison with the COMSOL simulations allows us to see that the convergence of the series is absolute.

Our incident beam propagating along y has an only z-component of the magnetic field (we denote its magnitude by A) and the incident electric field on the axis y is longitudinal:

$$H^i=H_z^i=A\sin(k\rho\sin\beta\sin\phi)e^{-jk\rho\cos\beta\cos\phi} \tag{1a}$$

$$E^i(\phi=0)=E_\rho^i=E_0e^{-jk\rho\cos\beta}, \tag{1b}$$

where $E_0=-jA\sqrt{\mu_0/\varepsilon_0}\sin\beta$.

For the mean electric intensity of the incident beam we have $I_0=E_0^2\sin^2(kR\sin\beta)/\sin^2\beta$. In the reported simulations $\beta=0.01$ and $\pi\ll kR<\pi/\beta$, i.e. an optically large cylinder is fully located in between two adjacent maxima of the incident beam. It implies that $E_0^2\ll I_0$.

If $kR\gg\pi$ any incident wave beam with any wave number k for any refractive index n of the cylinder efficiently excites in it a number of TM-polarized eigenmodes whose amplitudes are proportional to that of the incident beam. These eigenmodes (leaky as in any other dielectric cavity) resonate for given n at specific values of kR and for given kR at specific n. Every mode has a number of such resonances. We are looking for the regimes of the incident beam subwavelength focusing at the point ($\phi=0$, $\rho=R$). Subwavelength concentration of the electric energy implies the strong enhancement of the electric intensity $I=E_\rho^2$ at this point. What can cause this enhancement? Definitely, it may result from the resonances of the eigenmodes.

Therefore, we start from the study of the modal electric field excited by our beam at the point of our main interest ($\phi=0$, $\rho=R$) varying n and kR. Using the analytical solution, we calculated the partial intensities of the TM modes $E_{m\rho}^2$ excited by our beam at this point. These partial intensities, normalized to I_0, are shown in Fig. 2 as the functions of n for the case $kR=10$. In this case, the modes of the orders $m=11$–15 are resonant within the interval $n=[1.4,\ 2.0]$ where some resonances

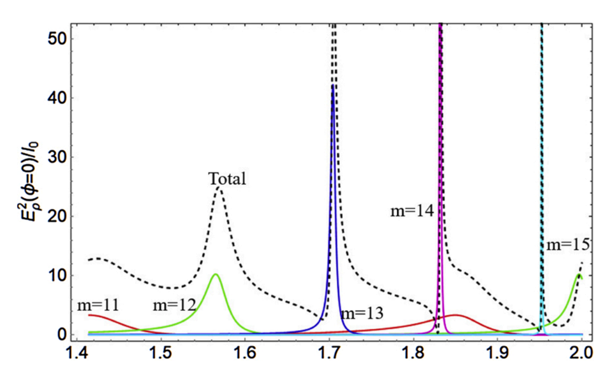

Fig. 2. Total (dashed line) and partial electric intensities of the eigenmodes ($m=11$ is red, $m=12$ is green, $m=13$ is blue, $m=14$ is magenta, $m=15$ is cyan) calculated at the point ($\phi=0$, $y=R$) for the case $kR=10$ versus the refractive index of the cylinder. All intensities are normalized to I_0.

are repeating. In the similar plots, calculated for larger kR, the density of the resonances of $E_{m\rho}^2$ over the axis n is higher because for the thicker cylinder the higher modes also become resonant. Similarly, the set of resonant regimes arises for given n versus normalized frequency kR and, similarly, the increase of n increases the density of the resonances on the axis kR.

Total intensity $I(0, R)$ results from the interference of these modes with one another and with the incident beam. However, as we can see in Fig. 2 $E_{m\rho}^2$ for $m = 11–15$ exceed I_0 for any n because the resonant ranges of n corresponding to different m intersect. Roughly speaking the whole range $n = 1.4–2$ is resonant for $kR = 10$. If we fix the refractive index, e.g. put $n = 1.7$ we will see that the whole range $kR = 10–20$ is resonant for it. Thus the feature of the resonant scattering is observed in the broad bands of the problem parameters.

Since $I_0 \gg E_0^2$ the intersecting resonances in Fig. 2 mean that $E_{m\rho}^2(0, R)$ exceeds the incident field intensity at the rear edge of the cylinder drastically. In other words, in the value $I(0, R)$ the contribution E_0^2 of the incident beam is negligibly small, and $I(0, R)$ is determined only by the interference of the excited eigenmodes. Studying the phases of these modes we have found that for $kR = 10$ the intensity $I(0, R)$ has local maxima versus n which do not exactly coincide with the resonant values of n seen in Fig. 2. And beyond these local maxima still the local field enhancement holds – $I/I_0 \gg 1$.

In Fig. 3 we present the plots of $I(\phi, R)/I_0$ calculated on the back side of the cylinder surface for (a) $n = 1.40$ and (b) $n = 1.57$. Analytical solution is in a very good agreement with the result of COMSOL in both cases. In Fig. 3(a) the angular width $\Delta\phi$ of the central intensity maximum determined in accordance to the Rayleigh criterion (0.7 of the maximum) is nearly 8.3°, that implies the linear width of the focal spot $R\Delta\phi \approx 0.24\lambda$. In Fig. 3(b) $\Delta\phi \approx 7.2°$ and the focal spot is narrower: $R\Delta\phi \approx 0.20\lambda$. In this case, the refractive index is close to the resonant values for the modes $m = 12$ and $m = 14$, and this is the reason why the focal spot for $n = 1.57$ is more subwavelength than it is for $n = 1.4$. Also, the local intensity enhancement at the focal point for $n = 1.57$ is as high as $22 - 24$ (24 results from the analytical model and 22 from COMSOL), whereas for $n = 1.4$ we have $I/I_0 \approx 11.5$ in both COMSOL and analytical solution. We have not found in the available literature, local intensity enhancement due to the presence of any dielectric cylinder of micron or submicron radius exceeding 4 for a point located in free space. It is clear that this effect results from a specific excitation of our cylinder.

The color map of the normalized intensity I/I_0 around the cylinder for the case $kR = 10$, $n = 1.4$ is presented in Fig. 4(a). The central focal spot with subwavelength width is not a waist of a photonic nanojet (see above). Together with two lateral spots the focal spot represents the birthplace of two wave beams symmetrically tilted to the axis y. A set of similar beams leaks from the overlapping spatial maxima of the important modes ($m = 11$, $m = 14$) on both sides of the cylinder. These lateral beams cannot be visually distinguished in the regions $|x| \geq 20$ where they become negligible on the background of the incident beam intensity maxima.

The most important feature we can see in this color map is a clear spatial separation of the central maximum (focal spot) from two lateral maxima. Also, it is seen that the focal spot keeps the subwavelength width at sufficiently small distances Δy from the rear edge of the cylinder. When $k\Delta y = 1$ (i.e. in the plane $ky = -11$) the linear width of the focal spot in the plane $(x - z)$ is nearly equal $\Delta x = 0.26\lambda$, i.e. is still subwavelength. For $n = 1.57$ the width of the focal spot at the same

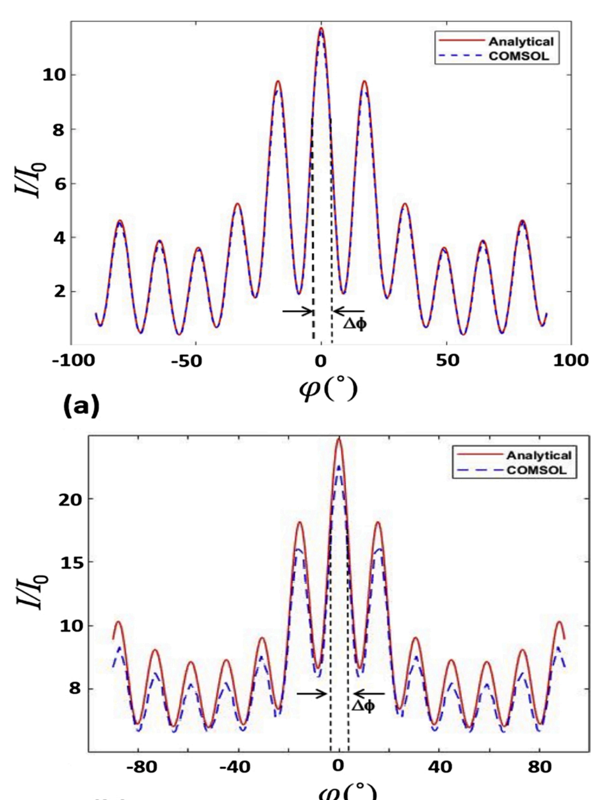

Fig. 3. Electric intensity enhancement on the back side of the cylinder for $n = 1.40$ (a) and $n = 1.57$ (b).

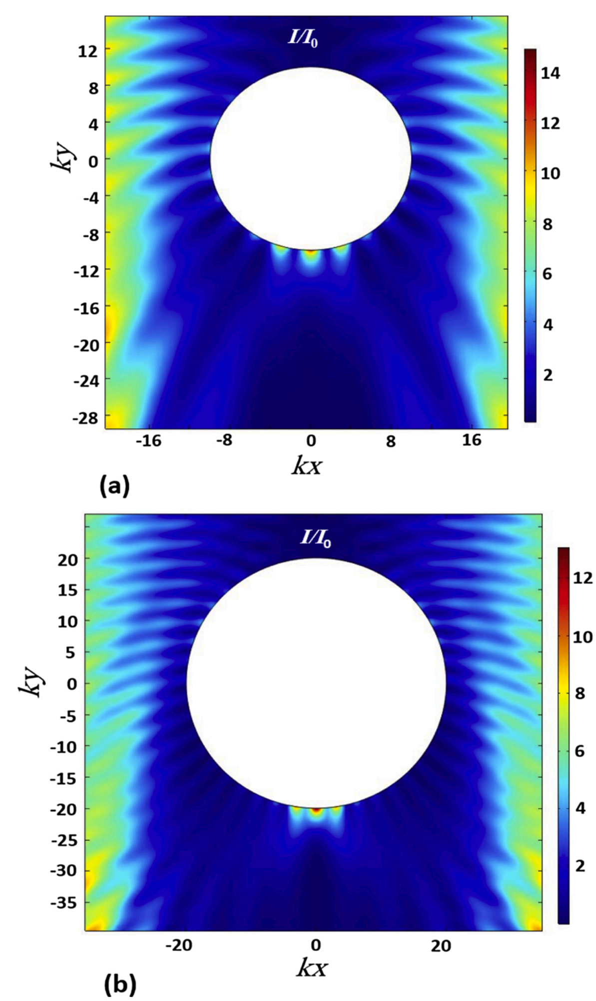

Fig. 4. Color map of the normalized intensity outside the cylinder when $kR = 10$, $n = 1.4$ (a) and the similar map when $kR = 20$, $n = 1.7$ (b). Incidence from top.

distance from the cylinder is smaller: $\Delta x = 0.22\lambda$. So, in a plane located at a certain distance from the microcylinder the intensity distribution still forms a pronounced subwavelength spot.

In Fig. 4(b) we present the similar color map for $kR = 20$ and $n = 1.7$. In this case, n is close to the resonant value, i.e. the regime is similar to the case $kR = 10$, $n = 1.57$. In this regime, $\Delta\phi \approx 4.7^\circ$. It implies the width of the focal spot at the cylinder surface $R\Delta\phi \approx 0.27\lambda$. At the distance $\Delta y = 1/k$ from the cylinder the width of the focal spot is $\Delta x \approx 0.29\lambda$ – still subwavelength and the intensity enhancement is still high – at the point ($x = 0$, $\Delta y = 1/k$ $I/I_0 = 9.5$.

Conventional focusing of a wave beam implies a symmetric interference pattern (of spatial harmonics composing the converging beam) distributed so that the intensity has the absolute maximum in the center of the focal spot (on the optical axis). The intensity distribution across the focal spot in the conventional case can be approximated as $I/I_0 \sim [\sin(\alpha x)/(\alpha x)]^2$. This is a qualitative (the so-called Kirchhoff) approximation, in which the parameter α depending on the focusing lens design determines the effective width of the focal spot. In the conventional case $\alpha < k$ and this width is larger than $\lambda/2$.

Let us discuss the difference of our interference pattern in our focal plane from the conventional focusing. First, our focal plane is given by $y = -R$, i.e. is plane tangential to the cylinder at its rear edge. Second, in Fig. 3 we see that the intensity is not nullified at the minima unlike the intensity of usual focused beam. In other words, the function of type $[\sin(\alpha x)/(\alpha x)]^2$ should be complemented by a weakly varying additive component (it tends to zero only for large x). Third, and this is most important, if we approximate the oscillating component of I/I_0 as $[\sin(\alpha x)/(\alpha x)]^2$, our α is larger than k. This is the indication of the contribution of the evanescent spatial spectrum. Of course, physically it is simply the implication of the resonant scattering when a TM-mode of the cylinder is excited inside it with the subwavelength intensity maxima (the length of the intensity maximum is nearly twice smaller than the distance $\lambda/2n$ between the adjacent intensity minima). However, in the usual case of the single-wave incidence the evanescent waves are confined inside the cylinder and these subwavelength features are hidden. Moreover, in the usual case there is no absolute central maximum. Engineering the interference of the mode patterns by the proper choice of the incident beam we achieve the absolute maximum at the axis and the extension of evanescent waves behind the cylinder. It results in the subwavelength focusing accompanied by high field concentration. This can be treated as a conversion of propagating waves in the spatial spectrum of the excited modes into evanescent waves.

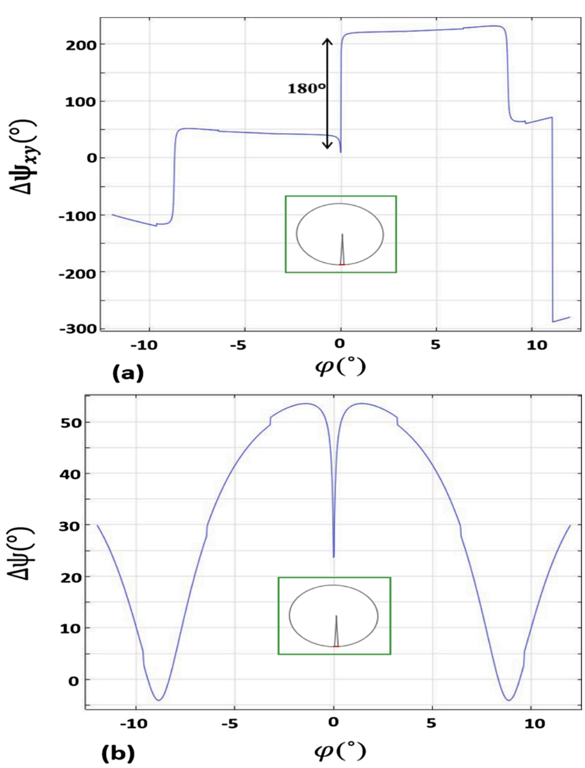

Fig. 5. (a) Distribution of the phase shift between E_x and E_y on the rear surface of the cylinder in a region covering three main local maxima of the electric field (this region is marked by red in the inset). (b) Phase shift between the electric and magnetic field vectors in the same area (b).

Fig. 5 illustrates the domination of the evanescent waves on the rear surface of the cylinder $kR = 10$, $n = 1.4$ via the analysis of the phase shifts between the components of the electromagnetic field. Fig. 5(a) depicts the distribution of the phase shift $\Delta\Psi_{xy}$ between two Cartesian components of the electric field over the part of the microparticle surface marked by red in the inset. This area covers the central focal spot and two lateral ones in which E_x and E_y have nearly the same magnitude. At the center of these spots the phase shift $\Delta\Psi_{xy} \equiv phase(E_x/E_y)$ passes through the values $\pm 90^\circ$ that means the circular polarization. In general, the electric polarization is elliptic. It is linear (and longitudinal) only on the axis y. Meanwhile the magnetic polarization keeps one-component polarization $H = H_z$ everywhere. The phase shift $\Delta\Psi$ between the elliptically polarized electric field vector and linearly polarized magnetic one exceeds 50° within the central spot. These phase relations and corresponding polarization transformation effect clearly point out the domination of the evanescent waves in the vicinity of the rear edge of our cylinder.

To conclude this subsection let us report the best corresponding result. Varying kR within the interval $10 \le kR \le 20$ and the refractive index in the limits $1.4 \le n \le 2$ we have found the case, when the linear width of the focal spot is minimal. This is the case when $kR = 20$ and $n = 1.610$. This refractive index is very close to the value $n = 1.612$ corresponding to the superposition of two resonances mode resonances: $m = 23$ and $m = 27$. The local intensity enhancement for this case is depicted in Fig. 6 in both color map and plot. The angular width of the focal spot on the surface is equal 3.1°, and the linear width is $R\Delta\phi \approx 0.15\lambda$. At the distance $\Delta y = 1/k$, i.e. in the plane $ky = -21$ the focal spot has the width $\Delta x \approx 0.16\lambda$. We can see that in this case our analytical solution and COMSOL simulations are also in a good agreement.

Thus, the possibility of subwavelength focusing of a diffraction free beam by a microcylinder is proved. This focusing is accompanied by a strong enhancement of the electric field in the focal spot. The subwavelength focusing can be implemented with several values of n for any kR if the adopted condition $\pi \ll kR \ll \pi/\beta$ is respected. For given n and R this regime can be implemented (under this condition) for several values of k. Therefore, a cosine wave beam with a wide enough continuous frequency spectrum impinging a glass microcylinder completely located between its intensity maxima contains the spectral components which will be focused behind the cylinder into a subwavelength spot.

2.2. Maximal enhancement of the surface-averaged electric intensity

Above it was shown that the resonant magnitudes of the eigenmode electric field at the point ($\phi = 0$, $\rho = R$) are achieved for a number of the cylinder parameters. The other sets of the design parameters offer the resonant magnitudes of the electric field at the other points of the cylinder surface. It is even possible to find the regime, when the value I/I_0 averaged over $-90^\circ < \phi < 90^\circ$ is maximized (for given kR or for given n). For $kR = 10$ the maximum of the mean value of I/I_0 (close to 15) is achieved when $n = 1.7$. This regime is illustrated by Fig. 7. We can see that the local maximum at the rear edge ($\phi = 0$, $\rho = R$) is relatively weak, whereas on the sides local intensity enhancement I/I_0 attains 23–24. The effective width of all local maxima is weekly subwavelength (close to 0.4λ). All intensity maxima except the axial one, in this regime can be treated as the waists of the photonic nanojets.

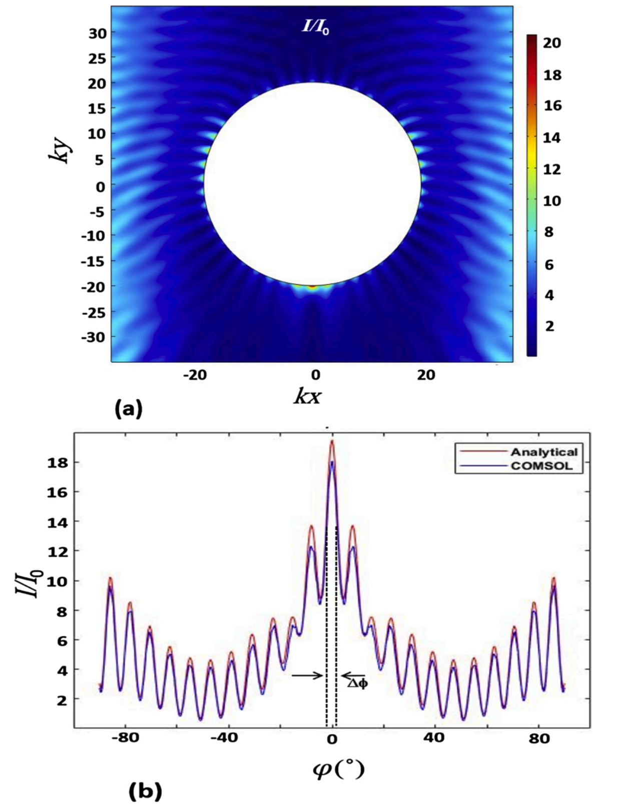

Fig. 6. Color map of the normalized intensity in the case of the tightest focusing, corresponding to $kR = 20$, $n = 1.61$ (a) and the plot of this intensity calculated on the back surface of the cylinder (b). Incidence from top.

Since this regime grants a significant enhancement of the electric intensity to the whole surface of the cylinder, it can be used for the enhancement of the fluorescence and Raman scattering of quantum emitters. For example, a long dielectric rod with optically substantial diameter can be covered by fluorescent molecules and impinged by a cosine beam. This technical solution will grant much higher level of the fluorescence than the well-known plasmonic fluorescent tag [10]. Really, the number of molecules coupled to a plasmonic nanoparticle is much smaller that the number of molecules covering a rod with the thickness of several microns – in our case the area is much larger. Meanwhile, the mean Purcell factor of a typical plasmonic fluorescent tag is of the same order of magnitude as in our case (10–20). The same observation concerns the surface-enhanced Raman scattering (SERS), because a substantial dielectric cylinder offers a large area for molecules emitting the Raman radiation. Our substantial cavity is also promising for SERS of biomedical objects chemically not compatible with metals and not detected therefore by usual metal SERS [11].

2.3. Eigenmode pattern in the case of the diffraction-free incident beam

In this subsection we discuss why the electric field in our case turns out to be strongly enhanced outside a dielectric microparticle, whereas in the case of a usual wave beam or a plane wave incident on any resonant dielectric microparticle a so drastic enhancement occurs only inside it.

Not only the internal field of the cylinder impinged by a wave beam comprises the cylindrical functions of high orders implying the small scale of spatial oscillations and, therefore, capable to grant the subwavelength field concentration due to their interference. The scattered field outside the cylinder comprises these functions as well. If we want to stress these terms, we may engineer the incident beam so that it would be nearly orthogonal to the large-scale oscillating terms and would maximally fit the small-scale ones. Our incident beam due to its symmetry does not excite the propagating waves in its paraxial region and, therefore, in this region the evanescent waves dominate. For small β the whole cylinder is located in this paraxial region, and the excited mode pattern is less leaky and more evanescent than in the case of a single-wave excitation.

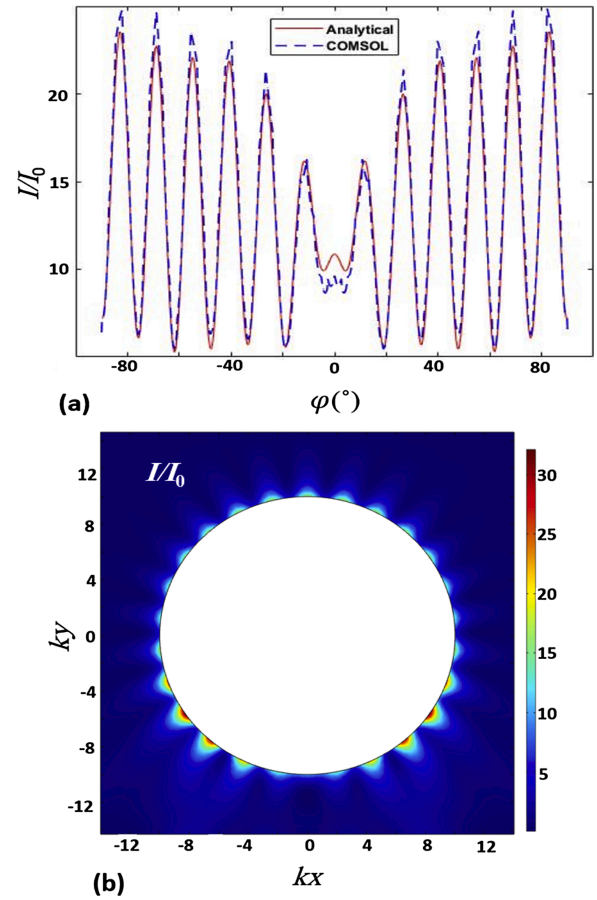

Fig. 7. Angular plot of the normalized intensity calculated on the back surface of a cylinder with $kR = 10$, $n = 1.7$ (a) and color map of intensity for the case (b).

We have studied our subwavelength effects for different values of β. For $\beta = 0.01$ (the case reported in the present paper) and for $\beta = 0.001$ all our results are practically the same. When $\beta = 0.1$ the values of the intensity enhancement reported above decrease nearly twice and the focal spots enlarge twofold. When $\beta = 0.2 > \pi/2kR$ the near-field effects beyond the cylinder practically disappear. In this trivial case, each of two incident plane waves independently generates its own photonic nanojet tilted to the axis y by angles $\pm\beta$.

Now, let us inspect the electric field pattern depicted in Fig. 8(a) for the case $\beta = 0.01$. We see that the spatial maxima of the electric field corresponding to the resonant mode $m = 13$ are extended in the radial directions and expand outside the cylinder. For a single plane wave incident along the same axis y the field maxima of the mode TM_{13} are nearly circular spots which do not expand outside. The magnetic field map depicted in Fig. 8(b) is not very different from that corresponding to the incidence of a single plane wave. Both shapes and sizes of the magnetic hot spots are visually the same. The main difference is the split of two magnetic field maxima centered at the axis y onto two spots with the exact zero between them because in the present case $H(\phi = 0) = 0$. For the magnetic field outside the cylinder we have not find near-field effects. Only the magnitude and phase of the outer electric field feel the impact of the resonances.

Thus, our beam of two plane waves with a small angle 2β between

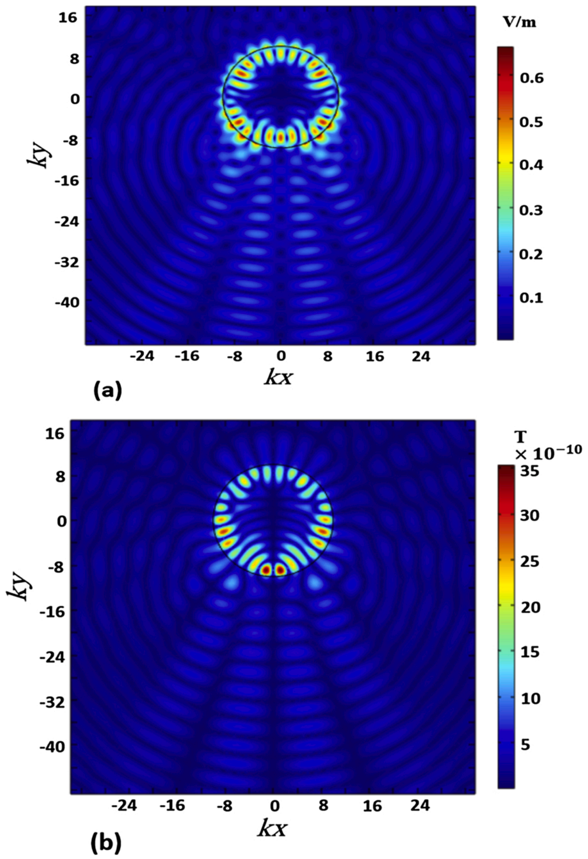

Fig. 8. Color map of the scattered electric field (instantaneous distribution of the magnitude) for the case $kR = 10$, $n = 1.7$ (a). Color map of the scattered magnetic field for the same case (b).

the wave vectors offers an interference effect of the resonant or nearly resonant eigenmodes induced in the microcylinder which drastically elongate the tails of the modal maxima and increase the impact of the evanescent waves behind the cylinder – on its surface and even at a small distance from it.

3. Conclusions

In this work we have studied the incidence of a fully symmetric diffraction-free beam on an optically thick dielectric cylinder. We designed the incident beam so that the electric and magnetic intensities have deep minima on its optical axis and the cylinder though very thick is fully located in between two adjacent maxima. For this case we theoretically revealed two strong effects of the local intensity enhancement. The novelty of the first effect is the location of the hot spot. It is located in free space and is centered by the rear edge of the cylinder. The plane tangential to the rear edge can be treated as a focal plane, and the corresponding field concentration can be treated as a subwavelength focusing. The second one is drastic enhancement of the electric intensity on the whole surface of the cylinder, especially high on its back side. The novelty of this effect is the large area where the field is enhanced. In the available literature the area of local field enhancement resulting from the resonant scattering by a dielectric cylinder is of the order of a wavelength (photonic nanojet) or smaller. In our case this area is as large as dozens of wavelengths, and the enhancement is much larger than in the case of a nanojet.

We have shown that in both cases the evanescent waves dominate over the propagating waves. The conversion of the incident propagating waves into evanescent ones in the area turns out to be so efficient, because the cylinder is located in the paraxial region of the incident beam having the exact zero at the optical axis. In this region, propagating spatial harmonics of the scattered field basically cancel one another that enhances the near-field effect. Of course, our effect is nothing but the interference of two conventional resonant scatterings. However, we do not claim a new physical mechanism of the local intensity enhancement. We claim the method of its engineering with the purpose to drag the hot spot of enhanced electric field from the cylinder to free space.

Now let us discuss possible applications. First, the subwavelength focusing can be utilized in the label-free far-field subwavelength imaging. In our work [12] we have shown that the microcylinder excited by a closely located radially polarized dipole creates a 2D Mathieu beam. In this work we show that another microcylinder focuses this beam into a small spot. Now all we need to achieve the subwavelength image of a point dipole is to combine these two cylinders locating the second one far from the first one. As to the second application, it refers to our second effect. As it was explained above, a large-area local intensity enhancement is promising for cavity-enhanced fluorescence [10] and cavity-enhanced all-dielectric Raman scattering [11]. We will be not surprised if our effects will find even more nanophotonic applications, than these two ones.

Declaration of Competing Interest

The authors report no declarations of interest.

Acknowledgement

Funding by the Russian Foundation for the Basic Research (grant N2-18-02-00315) is acknowledged by V.K.

Appendix A. Supplementary data

Supplementary data associated with this article can be found, in the online version, at https://doi.org/10.1016/j.photonics.2021.100894.

References

[1] Q.-X. Zhu, Description of the propagation of a radially polarized beam with the scalar Kirchhoff diffraction, J. Mod. Opt. 56 (2009) 1621–1625.
[2] E. Recami, M. Zamboni-Rached, L.A. Ambrosio, Non-Diffracting Waves, John Wiley Sons, Ltd, 2014.
[3] A.V. Osipov, S.A. Tretyakov, Modern Electromagnetic Scattering Theory with Applications, John Wiley Sons, Ltd, 2017.
[4] V. Kavungal, L. Bo, Q. Wu, T. Mianzhen, Study of whispering gallery modes in a cylindrical microresonator excited by a tilted fiber taper, SPIE Proceedings (2018).
[5] B.S. Luk'Yanchuk, Z.B. Wang, W.D. Song, M.H. Hong, Particle on surface: 3d-effects in dry laser cleaning, Appl. Phys. A 79 (2004) 747–751.
[6] A.V. Itagi, W.A. Challener, Optics of photonic nanojets, J. Opt. Soc. Am. A 22 (2005) 2847–2858.
[7] Z. Chen, A. Taflove, V. Backman, Photonic nanojet enhancement of backscattering of light by nanoparticles: a potential novel visible-light ultramicroscopy technique, Opt. Express 12 (2004) 1214–1220.
[8] A. Heifetz, S.-C. Kong, A.V. Sahakian, A. Taflove, V. Backman, Photonic nanojets, J. Comput. Theoret. Nanosci. 6 (2009) 1979–1992.
[9] R. King, W. Tai-Tsun, The Scattering and Diffraction of Waves, Harvard University Press, 1959.
[10] B. Valeur, M.N. Berberan-Santos, Molecular Fluorescence: Principles and Applications, Wiley-VCH, 2012.
[11] I. Alessandri, J.R. Lombardi, Editorial: surface enhanced Raman scattering: new theoretical approaches, materials and strategies, Front. Chem. 8 (2020) 63.
[12] R. Heydarian, K. Simovski, Role of the normal polarization in the far-field subwavelength imaging by a dielectric microsphere or microcylinder, J. Opt. 22 (2020) 075002.